# A Dynamic Pattern of Mechanical Stimulation Promotes Ossification in Avian Embryonic Long Bones

Niamh C. Nowlan <sup>1</sup>, Paula Murphy <sup>2</sup>, Patrick J. Prendergast <sup>1</sup>\*

- 1. Trinity Centre for Bioengineering, School of Engineering, Trinity College Dublin, Ireland
- 2. Department of Zoology, School of Natural Sciences, Trinity College Dublin, Ireland.

<sup>\*</sup>Address for correspondence: Patrick Prendergast, Trinity Centre for Bioengineering,
School of Engineering, Trinity College Dublin, Ireland, Phone: +353-1-896-3393; Fax: +353-6795554; E-mail: pprender@tcd.ie.

#### **Abstract**

We have performed a set of finite element analyses of embryonic chick hindlimb skeletal rudiments at several time points during development, around the time of initial bone formation. Using optical projection tomography, we created anatomically accurate rudiment and muscle morphologies for each stage. The change in pattern and magnitude of biophysical stimuli (such as stress, strain, hydrostatic pressure and fluid flow) were computed, and were found to change as mineralization and bone formation proceeded in the rudiment. For each biophysical stimulus, a single concentration of the stimulus was predicted at the mid-diaphysis some time before initial bone formation begins. Then, several hours before ossification, two concentrations of the stimuli were predicted distal and proximal to the prospective bone collar. Once bone formation had begun, high concentrations of the stimuli were maintained proximal and distal to the bone collar. We propose the hypothesis that patterns of biophysical stimuli resulting from mechanical loading due to muscle contractions initiate and propagate ossification in avian embryonic long bones, whereby a region of the perichondrium experiences a period of time under high cyclic stimulus levels, prompting mineralization and bone formation in this region some hours later.

**Keywords:** Mechanobiology, long bone development, finite element analysis, muscle contractions, periosteal bone collar.

#### 1. Introduction

Mechanical forces due to muscle contractions are important for normal embryonic bone growth (Palacios *et al.*, 1992). The embryonic chick has been used to study the influence of muscle contractions on embryonic skeletal growth (Nowlan *et al.*, 2007). In the chick, by 6 to 6.5 days of incubation, chondrocytes in the mid-diaphysis undergo hypertrophy, and by 6.5 to 7 days of incubation, bone collar formation begins in the mid region of the diaphysis with the deposition of osteoid below the perichondrium. The first mineralization takes place 0.5 to 1 days later in the form of laminae of bone which eventually fuse to form a thin, compact cylinder – the periosteal bone collar (Hall, 1987). Genes have been identified that direct or influence early limb bud formation, for example, the expression of the signalling molecules FGF10 and Wnt8c mark the site of hindlimb bud formation 6 hours before the limb bud becomes visible (Kawakami *et al.*, 2001). In the later developing limb bud, the initiation and progression of ossification is regulated in part by Indian Hedgehog (Ihh) and PTHrP signalling pathways (Vortkamp *et al.*, 1996). However, no explicit link between the mechanical forces generated by muscle contractions and the progression of ossification in the developing limb has yet been elucidated.

Several researchers have attempted to model the effect of mechanical forces due to muscle contractions using Finite Element (FE) analysis but, although a correlation between mechanical stimulation and ossification has generally been predicted in previous models, conflicting conclusions have been proposed. The results from Carter *et al.* (1987), who used a series of 2-D plane-strain FE models of the embryonic and post-natal femur, supported the hypothesis that ossification is accelerated by intermittently applied shear stresses and inhibited or prevented by intermittently applied hydrostatic pressure. Wong and Carter (1990b) performed an FE analysis of the *in* vitro culture study of embryonic mouse skeletal rudiments by Klein-Nulend at al. (1986), and suggest that

the increased mineralization rates observed in vitro were due to local shear stresses at the mineralization front induced by externally applied hydrostatic pressure. They modelled embryonic cartilage as having linear elastic (single phase) material properties, but when the analysis was repeated by Tanck et al. (1999) using poroelastic (fluid and solid phase) material properties, the same conclusion of shear stress stimulated ossification was not corroborated. In their 3D FE model, Tanck et al. (1999) found that distortional strains occurred in the region where mineralization proceeded, but concluded that the distortional (shear) strain was probably too small to have stimulated this. They concluded instead that the diffusion of ions as a result of the applied hydrostatic pressure itself may have enhanced the mineralization process in vitro. However, Tanck et al. (2000) returned to the hypothesis of strain-mediated mineralization in their FE analysis of the effect of embryonic muscle contractions at the mineralization front of a metatarsal rudiment and concluded that distortional strain rather than hydrostatic fluid pressure is a likely initiator of mineralization for in vivo embryonic bone growth. A number of further studies by Carter and co-workers have used a combination of the maximum octahedral shear stress and the minimum hydrostatic stress as mechanoregulators of endochondral ossification (Wong and Carter, 1990ab), in investigating the endochondral ossification of long bones (Stevens et al., 1999), and sesamoids (Sarin and Carter, 2000) and the formation of coxa valga in developmental dysplasia of the hip (Shefelbine and Carter, 2004). Heegaard et al. (1999) used local peak hydrostatic stress as a mechanobiological stimulus in their model of embryonic joint morphogenesis.

It is possible that the difficulty in discriminating between the various hypotheses relating to how mechanical forces modulate embryonic bone development is due to simplifications of the morphology, material properties and muscle loading schemes used in previous finite element models. In this paper, we use optical projection tomography to create a finite element model incorporating

realistic 3-D tissue morphologies for bone and more realistic representations of muscle loading. We use the model to test the hypothesis that patterns of biophysical stimuli resulting from mechanical loading due to muscle contractions initiate and propagate ossification in avian embryonic long bones. The quantitative nature of the model combined with its increased morphological accuracy allows quantification of biophysical stimuli active during bone formation in limb development.

## 2. Methods

FE analyses of embryonic chick hindlimb rudiments for a range of developmental stages before and during ossification were performed. Accurate 3D morphologies for skeletal rudiments were obtained and muscle loading magnitudes, locations and attachment sites were calculated from 3D data of the muscle masses and tendons present at each stage examined (Nowlan *et al.*, 2006). The chick embryo staging system developed by Hamburger and Hamilton (HH) (1992) was used. We have observed by histological staining that ossification begins in the tibiotarsus rudiment of the chick between stages HH32 and HH33; therefore we focused on the tibiotarsus rudiment at stages HH30, HH32 and HH34, corresponding to between approximately 7, 8 and 9 days of incubation. Two rudiments for each stage, (i.e., six bones), were modelled in total.

#### Data Collection

Optical Projection Tomography (OPT)

Optical Projection Tomography (OPT) (Sharpe *et al.*, 2002) constructs an image by measuring the amount of light transmitted or emitted by an object when light is shone upon it. A specimen is rotated through 360° and a series of snapshots taken at different angles are integrated, using a backprojection algorithm, to give a complete 3D image of the specimen. The resolution is 15µm (Sharpe

et al., 2002). OPT can be used to scan coloured specimens, such as those stained with histological stains or after an in situ hybridisation procedure. Specimens stained with fluorescent markers can also be scanned. OPT was used to obtain 3D data for cartilage, calcified tissue, muscle and tendon morphologies (Figure 1a-c). The specimens stained for cartilage and bone were scanned to obtain the morphology of the rudiments, and those stained for muscle and tendon used to estimate the magnitude, orientation and attachment sites of the muscle forces at each stage.

## Obtaining Tissue Morphologies

Cartilage and calcified tissue elements were stained using a modification (0.1% concentration of Alcian Blue instead of 0.015%) of the protocol described by Hogan *et al.* (1994), where Alcian Blue was used for staining cartilage, and Alizarin Red for calcified tissue (Figure 1a). At least ten specimens per stage were stained and scanned.

For the specimens stained for muscle and tendon, a minimum of two limbs for each of the three stages were analysed. Control (sense) probes were routinely included. Scleraxis, a bHLH (basic-Helix-Loop-Helix) transcription factor, has been identified as a highly specific marker for tendons and ligaments in the developing limb (Schweitzer *et al.*, 2001). The tendons in the developing limb were visualised by performing whole-mount in situ hybridisations (Wilkinson, 1992) using a probe for Scleraxis (chick EST database, clone ID ChEST654f15) (Figure 1b).

Differentiating muscle cells were stained by immunohistochemistry using a monoclonal antibody (MF20, Developmental Studies Hybridoma bank, 1/20 dilution) that specifically binds to a muscle specific protein, myosin (primary antibody) (Figure 1c). The presence of the anti-myosin antibody was subsequently detected by the binding of a fluorescently labelled secondary antibody (Alexa Fluor 488 goat anti-mouse IgG, Molecular Probes, 1/200 dilution, excitation and emission wavelengths 495 nm and 519 nm respectively).

## Finite Element Analysis

# Morphology

A 3D image VTK (Visualization Toolkit<sup>1</sup>) format was obtained from the OPT data for cartilage and calcified tissue. The VTK representation was imported into Rhino<sup>2</sup>, a modelling tool. Slices were taken of the VTK image, and the slices lofted to form a surface. This surface was then imported into CUBIT<sup>3</sup>, where it was meshed and converted to a format suitable for Abaqus<sup>4</sup> finite element software. This process is illustrated in Figure 2.

The 3D tendon and muscle data were examined, and the number of relevant muscles acting on the rudiments at each stage identified. The transverse cross-sectional area of each muscle was taken at the longitudinal mid–point of the muscle masses (Figure 1c-d), and the resultant force calculated using a force per unit area value for embryonic chick muscle of 1.11 mN/mm², as derived from Landmesser and Morris (1975). Muscle cross-sectional areas were measured for two specimens at each stage, and the values averaged for calculating the force. The attachment point for each muscle was located on the rudiment by visual comparison of the 3-D tendon data with a merged 3-D movie of the cartilage and muscle data at corresponding stages.

## *Material Properties*

At stages HH30 and HH32, the rudiment consists of cartilage only, while at Stage HH34 onwards, cartilage and calcified tissue are present (Fig 1a). As cartilage is a biphasic material, a poroelastic analysis was performed. Ten-node tetrahedral elements were used for the FE analysis, which was performed in Abaqus<sup>®</sup>. The mechanical properties calculated by Tanck *et al.* (2004) for the Young's modulus of unmineralized and mineralized embryonic mouse ribs were used, with the

<sup>1</sup> http://public.kitware.com/VTK, last accessed 22-01-2007

<sup>&</sup>lt;sup>2</sup> ©, http://www.rhino3d.com/, last accessed 22-11-2006

<sup>&</sup>lt;sup>3</sup> ©, http://cubit.sandia.gov/, last accessed 22-11-2006

<sup>&</sup>lt;sup>4</sup> ©, http://www.hks.com/, last accessed 22-11-2006

values from Tanck *et al.* (2000) for permeability and Poisson's ratio. The properties, for unmineralised and mineralized cartilage, are as follows: 1.1 MPa and 117 MPa for Young's modulus [E],  $6.7 \times 10^{-15}$  m<sup>4</sup>/N.s and  $6.7 \times 10^{-16}$  m<sup>4</sup>/N.s for permeability (k) and 0.25 and 0.30 for Poisson's ratio [v], respectively. The calcified cartilage collar was modelled as a shell which extends into the rudiment to a thickness of 0.1 mm, a figure obtained by the depth of Alizarin Red staining in transverse cryostat sections of tibiotarsi (not shown).

## **Boundary Conditions**

Following Tanck et al. (2000), one loading cycle consisted of two muscle twitches, a flexion contraction followed by an extension contraction where each twitch lasted for 1.4 seconds which includes ramp up, hold and ramp down phases. As also described in that study, it was assumed that during the flexion contractions, each muscle on the ventral aspect of the rudiment was activated, while during the extension contraction the muscles on the dorsal aspect were activated. This has been shown to be the case in avian embryonic development, between seven and nine days of incubation (Bekoff, 1976). The force of each muscle transmitted by the adjoining tendons was estimated as being spread over an element face at the distal end of the rudiment in the form of a surface traction. Two of the nodes at the proximal end of the rudiment were restrained from movement, while the rest of the nodes at the proximal end were restrained in the vertical direction only. A spring was attached to a rigid plate connected to the distal end of the rudiment to simulate the restraint of the opposing joint, as illustrated in Figure 3. The stiffness of the spring was calculated as that of an opposing block of cartilage of varying height according to stage, as detailed in Table 1. A zero pore-pressure boundary condition was specified on all the external nodes of the rudiment, thereby allowing fluid flow out of the structure. For each analysis, the following parameters were computed; maximum principal stress, maximum principal strain, octahedral strain, relative fluid-solid velocity and

hydrostatic pressure. A stimulus (S) was defined, following Prendergast *et al.* (1997), as a combination of the shear strain and fluid velocity, as defined by

$$S = \frac{\gamma_{oct}}{a} + \frac{v}{b}$$

where a = 0.0375, and  $b = 3 \mu m s^{-1}$ .

## 3. Results

#### 3.1 Muscle Forces

The forces were calculated for ventral and dorsal muscles at stages HH30, HH32 and HH34 as shown in Table 2. By HH34, the force exerted by the ventral muscles was found to increase to 0.962 mN, and by the dorsal muscles to 0.607 mN.

# 3.2 Comparison between specimens

Morphological analyses were carried out, and two specimens that were typical for each stage were chosen for FE analysis. The length of these rudiments was, on average, 2.3mm at stage HH30, 4.2mm at HH32 and 5.7mm at HH34. The FE analysis for two specimens at each stage showed that, although peak values did not correlate exactly between specimens, the patterns of mechanical stimuli were very similar, as shown in a comparison of fluid velocity, and maximum principal stresses for specimens A and B at stage HH34 (Figure 4). Therefore, in order to avoid repetition, the results shown in the following sections are from one set of specimens (Set A), but the patterns have been corroborated in a second complete set. The results are presented as a series of dorsal and/or ventral views at the mid time-point of the flexion and extension contractions, i.e., 0.7 seconds into each contraction.

## 3.3 Comparison between aspects and contractions

The stress, strain, octahedral strain and fluid velocity differed in some respects as regards relative levels of concentration during different contractions, or between ventral and dorsal aspects, as shown for a single FE analysis of a HH32 rudiment in Figure 5. With stress and strain, the concentrations reached higher values on the opposite side to load application; i.e., higher on the dorsal aspect during the flexion contraction (in which the load is applied ventrally) and on the ventral aspect during the extension contraction (Fig. 5a-c). Octahedral strain tended to be highest during the flexion contraction on the ventral aspect than at any other time during the loading cycle (Fig. 5b), and the fluid velocity also reached higher levels on the ventral aspect during both contractions (Fig. 5d). The fluid velocity profiles did not follow the load application profiles exactly, with a low point occurring before the load goes to zero in between the two contractions (data not shown). Stress values tended to be very low on the aspect of load application (Fig. 5c). During the flexion contraction, hydrostatic pressure was positive on the ventral aspect and negative on the dorsal aspect, while during the extension contraction the opposite was true. At HH32, the stimuli were concentrated at the proximal end of the rudiment during the extension contraction (Fig. 5a-d).

During the loading cycle, stress and strain values were at a maximum throughout the 'hold' phase, while fluid velocity, hydrostatic pressure and stimulus (S) peaked at the top of the first ramp phase of each contraction.

## 3.4 Comparison between stages

All stimuli changed in pattern and magnitude as the rudiment grows and develops. Within each stage, the patterns obtained for the maximum principal stress ( $\sigma_1$ ), maximum principal strain ( $\varepsilon_1$ ), octahedral shear strain ( $\gamma_{\text{oct}}$ ) fluid velocity ( $\nu$ ) and stimulus (S) were quite similar to each other (Figure 6). In the earliest stage examined, HH30, concentrations of each of these variables occurred at the mid-diaphysis. Later, at HH32, although the rudiment was still composed only of cartilage, a

slight bulge was present at the mid-diaphysis (indicated by arrow on Fig. 6a). This caused the concentration of biophysical stimuli to relocate distal and proximal to the mid-diaphysis, giving two distinct concentrations above and below the site where the periosteal bone collar would *later* form (HH32, Fig. 6a-d). The pattern was extended at stage HH34, with concentrations located even more proximally and distally to where the bone collar had now formed.

When the fluid velocity and octahedral shear strain at the surface were plotted along the length of the rudiments (for a path along the ventral surface of the rudiments), both separately and combined as the stimulus *S*, dynamic changes in stimuli become more evident. At HH30, one peak at the middiaphysis is predicted. At HH32 two peaks distal and proximal to the middiaphysis are predicted, where the value of the stimulus at the mid-point however is similar to that at HH30. At HH34, much larger and more separated peaks are predicted, with very low stimulus values at the middiaphysis (Fig. 7). At HH34, the peak values of stimuli were higher at the proximal end of the rudiment (Fig. 7a-d). Peak values for each of the stimuli increased by an average of 5.5 fold over the three stages, as shown in Table 3.

# 4. Discussion

All of the mechanical stimuli examined showed dramatic changes in pattern as mineralization and bone formation proceed in the rudiment. At the earliest stage examined, (HH30), stress, strain (maximum principal and octahedral shear), hydrostatic pressure and fluid velocity were at a high level of concentration at the mid-diaphysis of the long bone rudiment at the location where the periosteal bone collar will begin to form 1-1.5 days later. At approximately HH32, the diameter of the rudiment at the mid-diaphysis expands, probably due to hypertrophy of the chondrocytes in this region. This leads to an instability whereby the single region of concentration of biophysical stimuli

separated into two locations proximal and distal to the site of the future bone collar. After the bone collar appeared (HH34), the concentrations peaked proximal and distal to the bone collar. This means that stress, strain and fluid velocity levels were highest at locations where the bone collar would form some time later. We propose that high cycles of stimulus occur in the cartilaginous tissue as a promoter of ossification, where the cyclic nature of the stimulus is due to muscle contractions. A delay between patterns of high stimulus levels and bone collar formation indicates that mechanical stimuli are either influencing events prior to mineralization— they may stimulate chondrocyte hypertrophy— or that a time-lag exists between peak mechanical stimuli levels and the response of the perichondrium.

Some simplifications included in the analysis may have influenced the outcome of the model. Each muscle load was approximated as being distributed over an element face whereas, in reality, the tendon is inserted into the rudiment tissue. This simplification caused peak concentrations at the load application sites for stress and strain, as seen in Figure 5a-c. However, these additive peaks were at the proximal end of the rudiment, distant from the mid-diaphyseal region of interest. Furthermore, the material properties used were for murine embryonic cartilage and calcified cartilage rather than for avian tissues, as avian properties have not yet been measured. Constant material properties were used for the cartilage in the rudiment, and while it has been shown that the late-hypertrophic zone in rabbit growth plates has a higher Young's Modulus than the reserve zones (Radhakrishnan *et al.*, 2004), without similar testing of avian tissues, it cannot be assumed that avian growth plate material properties vary in a similar fashion. In addition, the cross-sectional areas of the muscle masses were calculated assuming that the muscle fibres were parallel. However, although different material properties or muscle force magnitudes may change the magnitudes of the stimuli, the resultant patterns will not be significantly altered.

It should be noted that the chick skeletal development differs from that of mammals. Avian long bones have no primary endochondral ossification centre and form bone tissue primarily via periosteal ossification (Fell, 1925). Therefore, the analyses presented here do not address endochondral ossification per se, but are relevant to events that are shared by birds and mammals and precede mammalian endochondral ossification, such as chondrocyte hypertrophy and periosteal ossification.

The results of the analyses suggest that we revisit some of the hypotheses published previously. The epigenetic influences of mechanical forces have often been considered as having a direct relationship to cell differentiation; for example, Wong and Carter (1990b) suggested that high shear stress values lead to accelerated osteogenesis while Tanck et al. (2000) proposed that high strain values at the periphery of an embryonic rudiment increase the mineralization rate. Our results suggest a more complex relationship, where a cyclic pattern of stimulus levels is established which predisposes bone formation at a later time. It is possible that the decreased cyclic stimulus levels at the mid-diaphysis due to expansion of the cartilaginous rudiment in this region could trigger the ossification progress; where these stimulus levels result from a bending moment induced by cyclic muscle forces.

In this study we set out to test the hypothesis that mechanical forces due to muscle contractions initiate and propagate periosteal ossification. We created a set of FE analyses at three different timepoints with a high level of accuracy for the geometry and loading conditions. A cycle of fluctuations of stress, strain, hydrostatic pressure and fluid flow concentrations were found on the perichondrium in regions of the rudiment that form bone sometime later, a number of hours before this ossification occurs. The results imply that, in order for a region to undergo ossification, levels of cyclic mechanical stimuli must be experienced in this region at a high level a number of hours in advance of mineralization. Our results are consistent with the view that a sustained period of cyclic

stress promotes chondrocyte hypertrophy; therefore stimulating mineralization and subsequent bone collar formation.

# Acknowledgements

This research was funded by the Irish Research Council for Science, Engineering and Technology (IRCSET) under the National Development Plan (NDP). The authors are grateful to Mr. Damien Byrne and Dr. Alex Lennon from the Trinity Centre for Bioengineering and Ms. Kristen Summerhurst from the Zoology Department, Trinity College Dublin and to Dr. James Sharpe from the Centre for Genomic Regulation, Barcelona for their advice on this research.

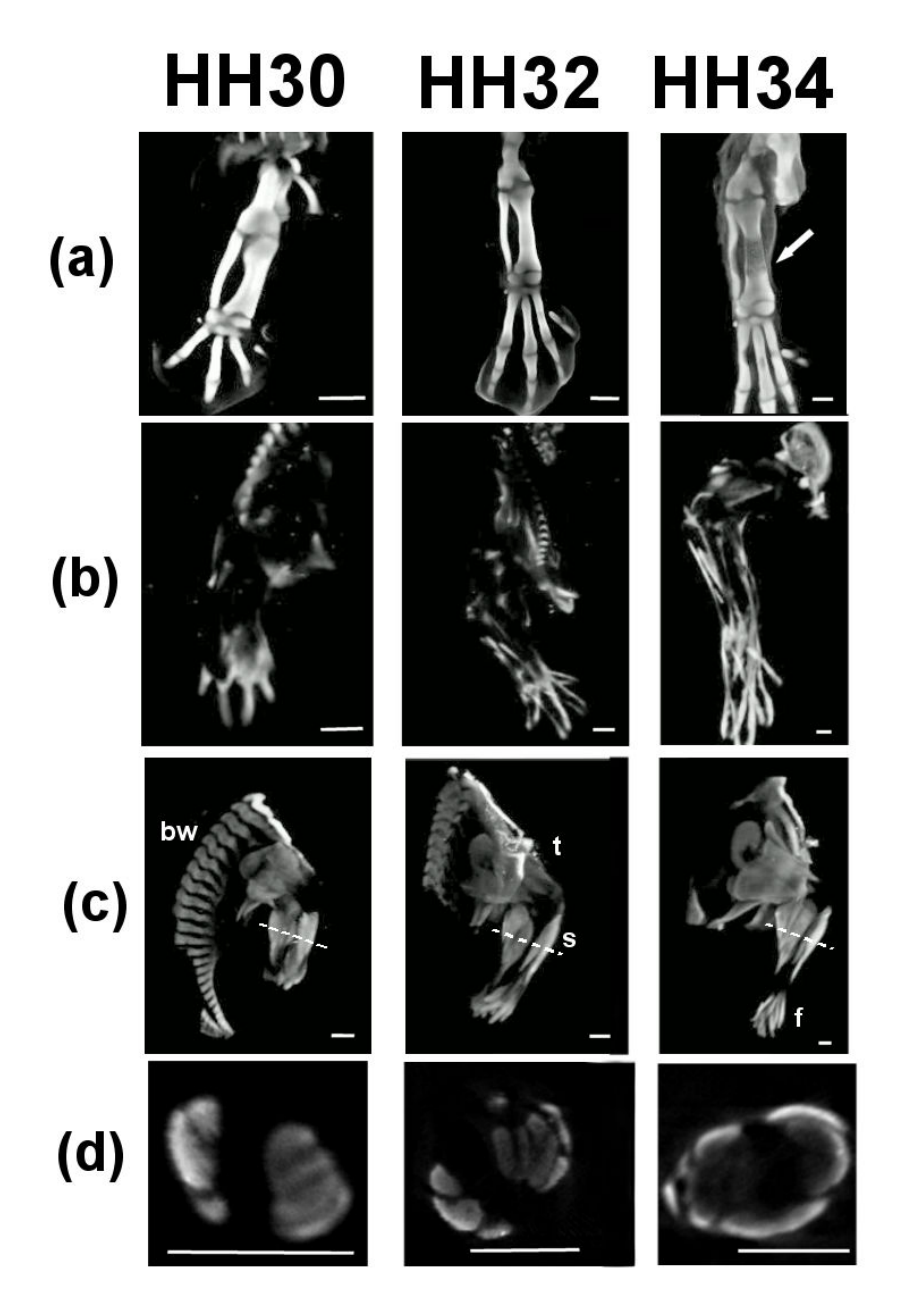


Figure 1: Stills from 3D scans of stained tissues at stages HH30, HH32 and HH34. Scale bars approximately 1mm. (a): cartilage (alcian blue), note the darker area (arrow) at the midpoint of the tibiotarsus indicating the first appearance of the bone collar (b): tendon (Scleraxis in situ), (c): muscle (anti-myosin antibody) with planes at which cross-sections were taken, 'bw' indicates body wall, 't' thigh, 's' shank and 'f' footplate muscles masses (d): cross-sections of muscle data from which muscle forces were calculated.

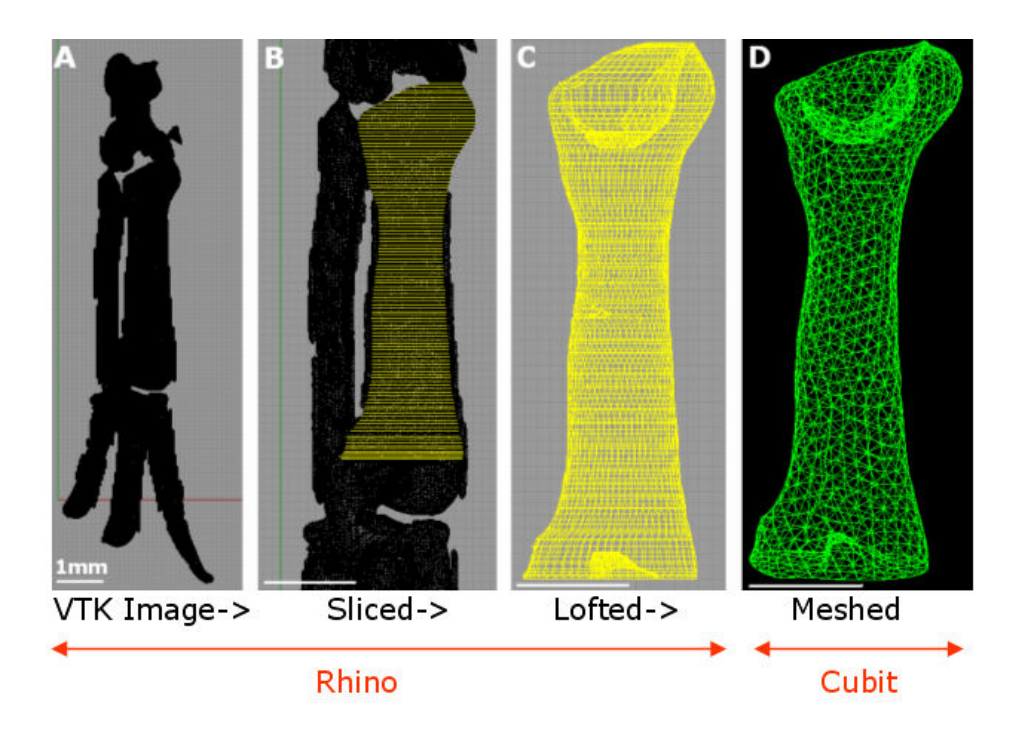


Figure 2: A 3D image from the OPT scan was sliced and lofted in Rhino, and the resulting shape meshed in Cubit.

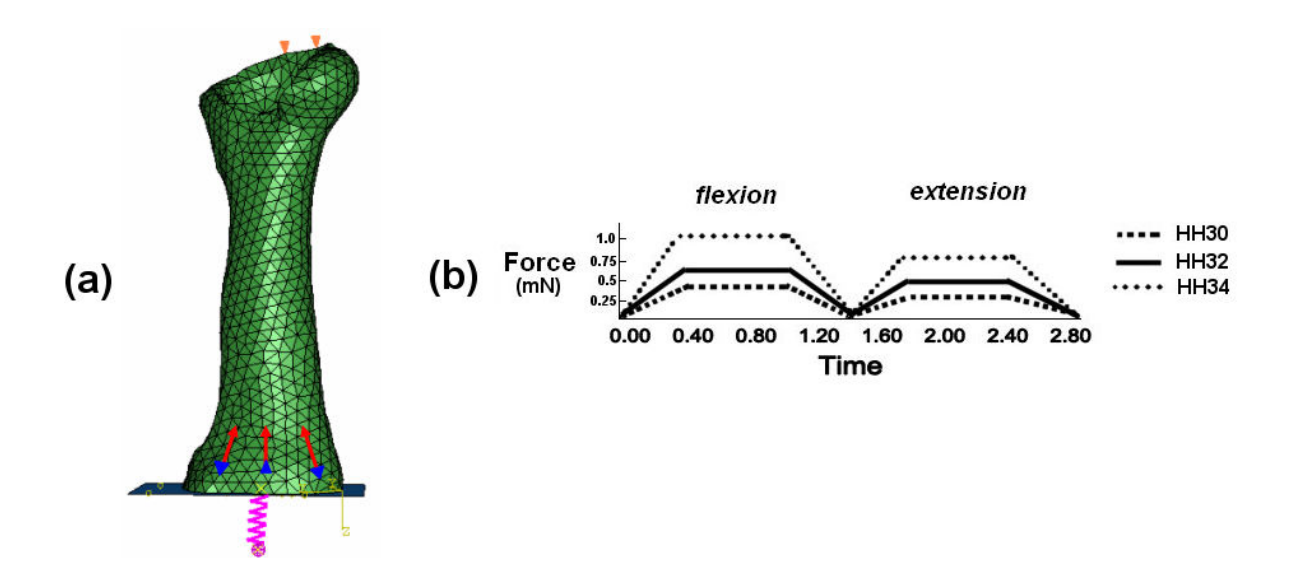


Figure 3: Illustration of distal spring restraint, fixed nodes, loads for flexion contraction at HH32, and (below) Loading regimes for HH30, HH32 and HH34.

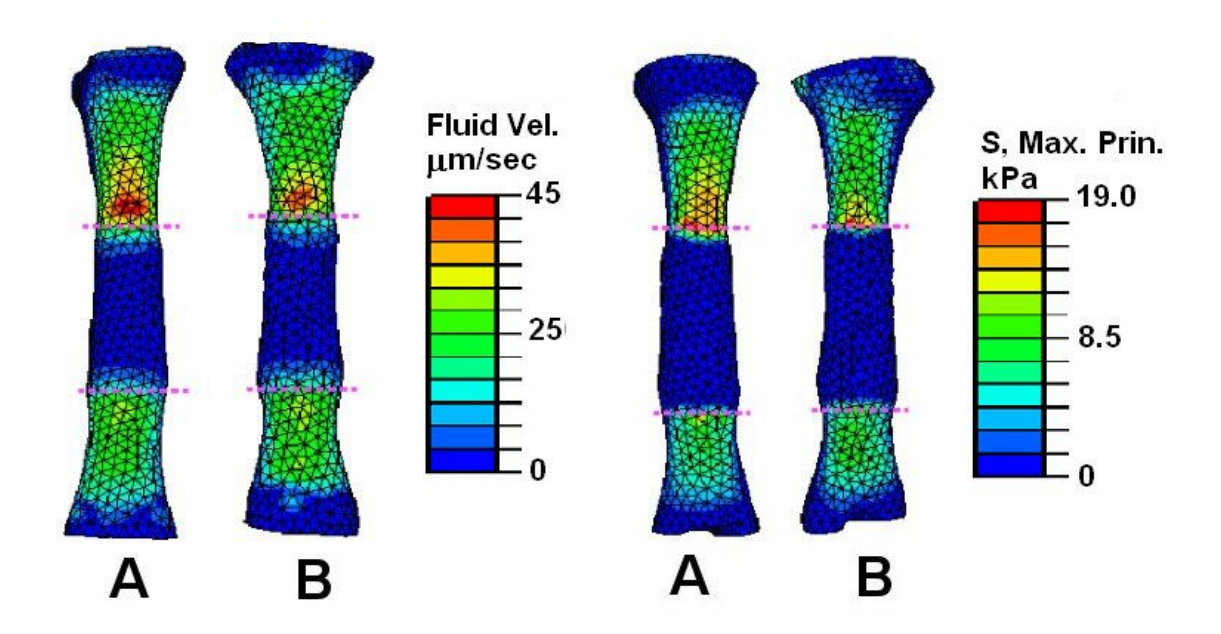


Figure 4: Comparison of fluid velocity (ventral aspect) and maximum principal stress (dorsal aspect) for specimens A and B at stage HH34. Dashed line indicates length of bone collar.

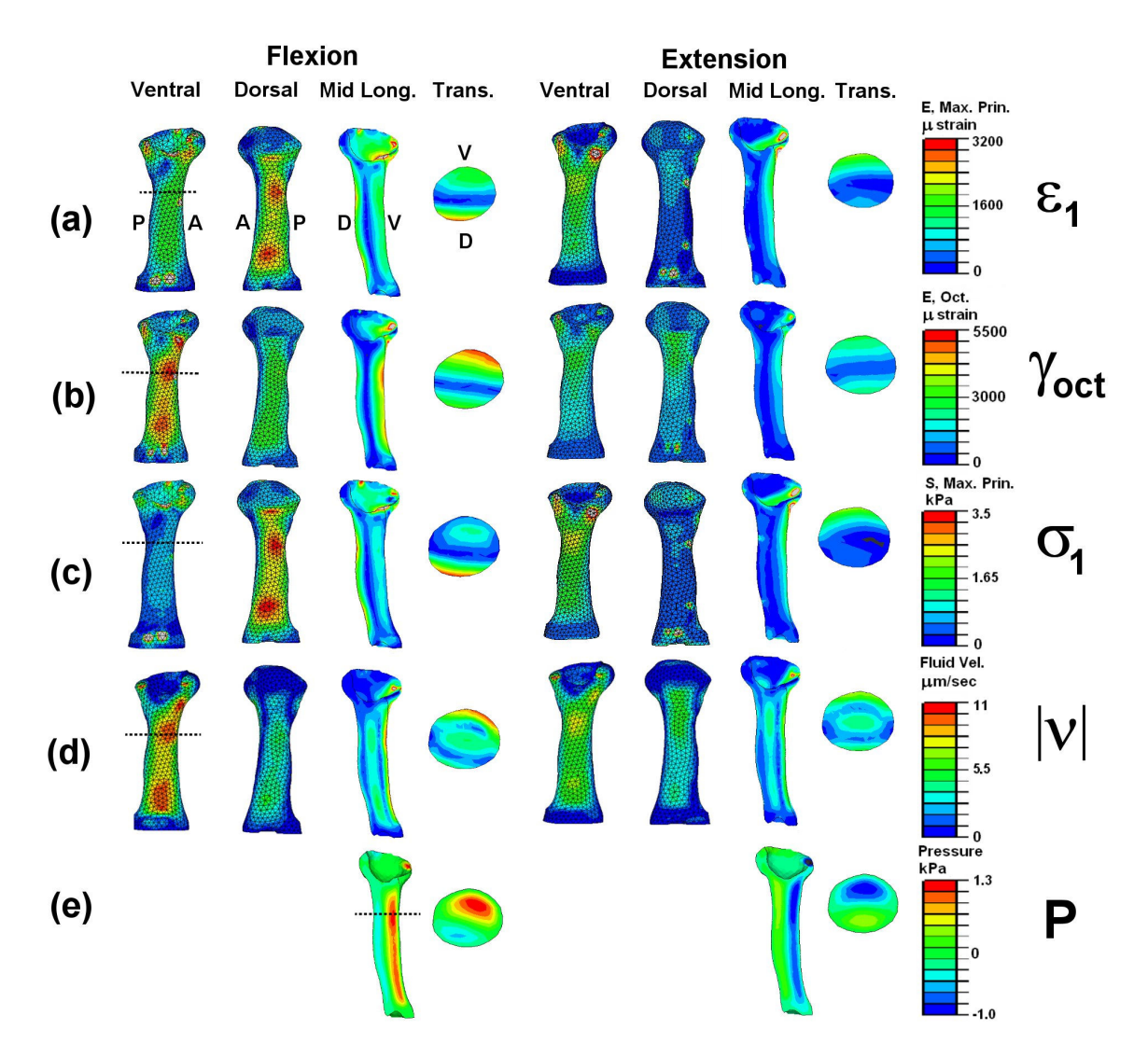


Figure 5: FE analysis results for HH32 mid-flexion and mid-extension contractions, ventral, dorsal, mid-longitudinal (Mid. Long.) section and transverse (Trans.) section views (transverse sections taken at level illustrated by dashed line. Proximal is up, distal is down. During flexion, loads are applied on the ventral aspect, and during extension on the dorsal aspect. 'A' represents anterior, 'P' posterior, 'V' ventral and 'D' dorsal. Views for all representations as detailed in (a).

(a): Maximum principal strain (µstrain), (b): Octahedral strain (µstrain), (c): Maximum principal stress (kPa), (d): Fluid velocity (µm/sec), (e): Hydrostatic pressure (kPa).

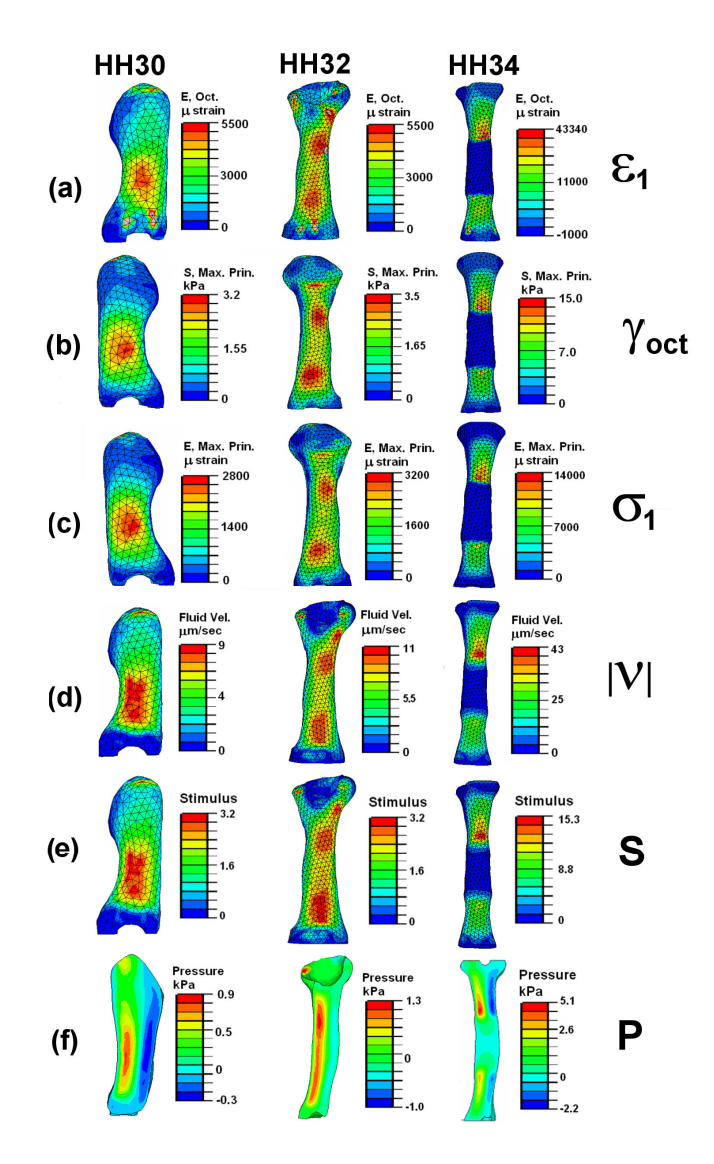


Figure 6: Mechanical stimuli patterns at HH30, HH32 and HH34, mid-flexion contraction. Arrow in (a) indicates bulge at mid-diaphysis at HH32.

- (a): Maximum principal strain (µstrain), dorsal aspect.
- (b): Octahedral strain (µstrain), ventral aspect,
- (c): Maximum principal stress (kPa), dorsal aspect,
- (d): Fluid velocity (µm/sec), ventral aspect,
- (e): Stimulus, ventral aspect,
- (f): Hydrostatic pressure (kPa), midline longitudinal section.

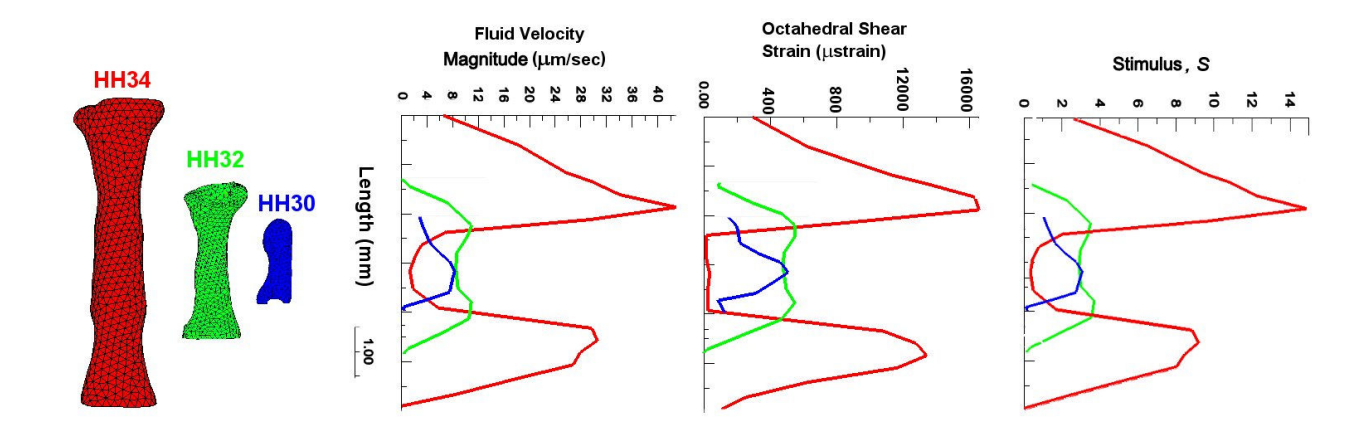


Figure 7: Comparison of fluid velocity, octahedral shear strain and stimulus values mid-flexion along the length of the ventral aspect of rudiments at HH30, HH32 and HH34.

#### References

- Bekoff, A., 1976. Ontogeny of leg motor output in the chick embryo: a neural analysis. Brain Res 106, 271-91.
- Carter, D. R., Orr, T. E., Fyhrie, D. P., Schurman, D. J., 1987. Influences of mechanical stress on prenatal and postnatal skeletal development. Clin Orthop Relat Res 15, 237-50.
- Fell, H. B., 1925. The histogenesis of cartilage and bone in the long bones of the embryonic fowl.

  Journal of Morphology and Physiology 40, 417-459.
- Hall, B. K., 1987. Earliest evidence of cartilage and bone development in embryonic life. Clin Orthop Relat Res 225, 255-72.
- Hamburger, V., Hamilton, H. L., 1992. A series of normal stages in the development of the chick embryo. 1951. Dev Dyn 195, 231-72.
- Heegaard, J. H., Beaupré, G. S., Carter, D. R., 1999. Mechanically modulated cartilage growth may regulate joint surface morphogenesis. J Orthop Res 17, 509-17.
- Hogan, B., 1994. Manipulating the mouse embryo: a laboratory manual. Cold Spring Harbour Laboratory, Cold Spring Harbor (NY).
- Kawakami, Y., Capdevila, J., Buscher, D., Itoh, T., Rodriguez Esteban, C., Izpisua Belmonte, J. C., 2001. WNT signals control FGF-dependent limb initiation and AER induction in the chick embryo. Cell 104, 891-900.
- Klein-Nulend, J., Veldhuijzen, J. P., Burger, E. H., 1986. Increased calcification of growth plate cartilage as a result of compressive force in vitro. Arthritis Rheum 29, 1002-9.
- Landmesser, L., Morris, D. G., 1975. The development of functional innervation in the hind limb of the chick embryo. J Physiol 249, 301-26.

- Nowlan, N. C., Murphy, P., Prendergast, P. J., 2006. The influence of mechanical forces in the growing embryonic limb. In Transactions of the 52nd Annual Meeting of the Orthopaedic Research Society. Chicago, Illinois [CD-ROM].
- Nowlan, N. C., Murphy, P., Prendergast, P. J., 2007. Mechanobiology of embryonic limb development. Ann N Y Acad Sci 1101, 389-411.
- Palacios, J., Rodriguez, J. I., Ruiz, A., Sanchez, M., Alvarez, I., DeMiguel, E., 1992. Long bone development in extrinsic fetal akinesia: an experimental study in rat fetuses subjected to oligohydramnios. Teratology 46, 79-84.
- Prendergast, P. J., Huiskes, R., Soballe, K., 1997. Biophysical stimuli on cells during tissue differentiation at implant interfaces. J Biomech 30, 539-548.
- Radhakrishnan, P., Lewis, N. T., Mao, J. J., 2004. Zone-specific micromechanical properties of the extracellular matrices of growth plate cartilage. Ann Biomed Eng 32, 284-91.
- Sarin, V. K., Carter, D. R., 2000. Mechanobiology and joint conformity regulate endochondral ossification of sesamoids. J Orthop Res 18, 706-12.
- Schweitzer, R., Chyung, J. H., Murtaugh, L. C., Brent, A. E., Rosen, V., Olson, E. N., Lassar, A., Tabin, C. J., 2001. Analysis of the tendon cell fate using Scleraxis, a specific marker for tendons and ligaments. Development 128, 3855-66.
- Sharpe, J., Ahlgren, U., Perry, P., Hill, B., Ross, A., Hecksher-Sorensen, J., Baldock, R., Davidson, D., 2002. Optical projection tomography as a tool for 3D microscopy and gene expression studies. Science 296, 541-5.
- Shefelbine, S. J., Carter, D. R., 2004. Mechanobiological predictions of growth front morphology in developmental hip dysplasia. J Orthop Res 22, 346-52.

- Stevens, S. S., Beaupré, G. S., Carter, D. R., 1999. Computer model of endochondral growth and ossification in long bones: biological and mechanobiological influences. J Orthop Res 17, 646-53.
- Tanck, E., Blankevoort, L., Haaijman, A., Burger, E. H., Huiskes, R., 2000. Influence of muscular activity on local mineralization patterns in metatarsals of the embryonic mouse. J Orthop Res 18, 613-9.
- Tanck, E., Van Donkelaar, C. C., Jepsen, K. J., Goldstein, S. A., Weinans, H., Burger, E. H., Huiskes, R., 2004. The mechanical consequences of mineralization in embryonic bone. Bone 35, 186-90.
- Tanck, E., van Driel, W. D., Hagen, J. W., Burger, E. H., Blankevoort, L., Huiskes, R., 1999. Why does intermittent hydrostatic pressure enhance the mineralization process in fetal cartilage? J Biomech 32, 153-61.
- Vortkamp, A., Lee, K., Lanske, B., Segre, G. V., Kronenberg, H. M., Tabin, C. J., 1996. Regulation of rate of cartilage differentiation by Indian hedgehog and PTH-related protein. Science 273, 613-22.
- Wilkinson, D. G., 1992. Whole mount in situ hybridization of vertebrate embryos. In: Wilkinson, D. G. (Ed.) In situ hybridization: A Practical Approach IRL Press, Oxford, pp. 75-83.
- Wong, M., Carter, D. R., 1990a. A theoretical model of endochondral ossification and bone architectural construction in long bone ontogeny. Anat Embryol (Berl) 181, 523-32.
- Wong, M., Carter, D. R., 1990b. Theoretical stress analysis of organ culture osteogenesis. Bone 11, 127-31.